

Supporting Information
for

**Database Analysis of Transition-Metal Carbonyl Bond
Lengths: Insight into the Periodicity of π Back-Bonding, σ
Donation, and the Factors Affecting the Electronic Structure of
the TM-C \equiv O Moiety**

Rosalie K. Hocking*,[†] and Trevor W. Hambley*

*Centre for Heavy Metals Research, School of Chemistry, University of Sydney, Sydney,
NSW 2006, Australia*

Experimental Methods

Excluding non-terminal modes of carbonyl bonding

In a manner similar to that described previously for carboxylates^{1,2}, non-terminal modes of carbonyl bonding were excluded by specifying coordination numbers of the carbon and oxygen atoms. The coordination number of the carbon was specified as two (oxygen and the metal), and that of the oxygen as one (the carbon), thus excluding the binding modes illustrated in Figure S1.

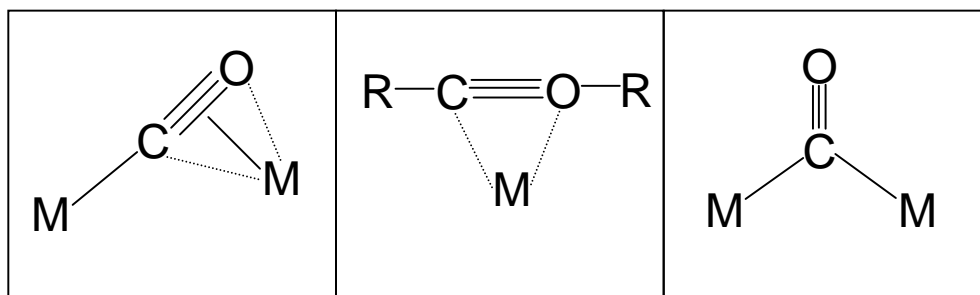


Figure S1. Examples of non-terminal modes of carbonyl bonding that have been excluded from the analysis.

Analysis

Scatter plots for all data.

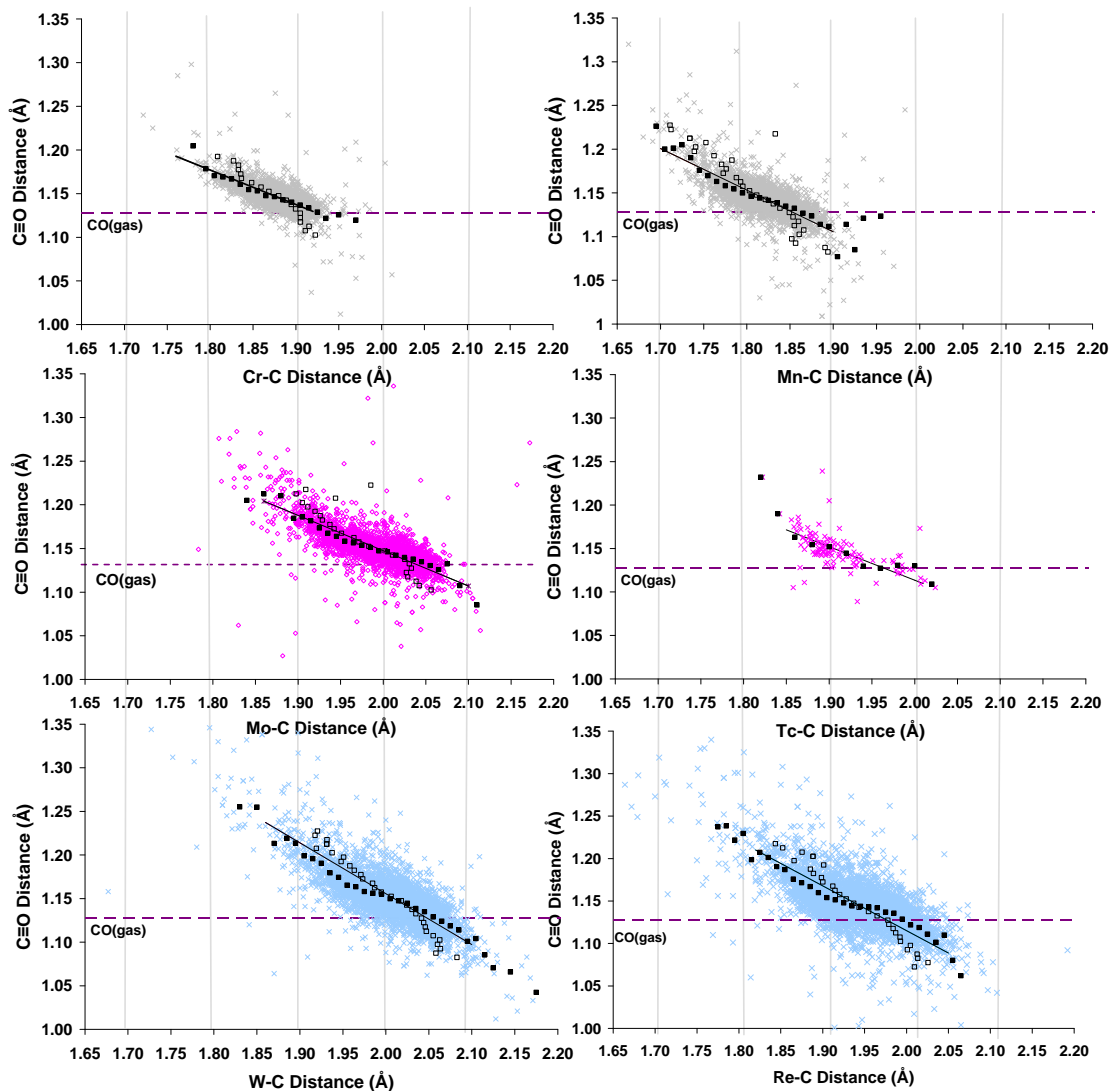


Figure S2. Scatter plot of C≡O distance vs. TM-C distance. Superposed are the weighted averages, the mean C≡O distance for a given TM-C distance $\{\bar{x}(C\equiv O|TM-C)\}$ (■), $\bar{x}(TM-C|C\equiv O)$ (□), and the principal component analysis (—) for groups 6 and 7. Grey lines are intended to reference the graphs to each other.

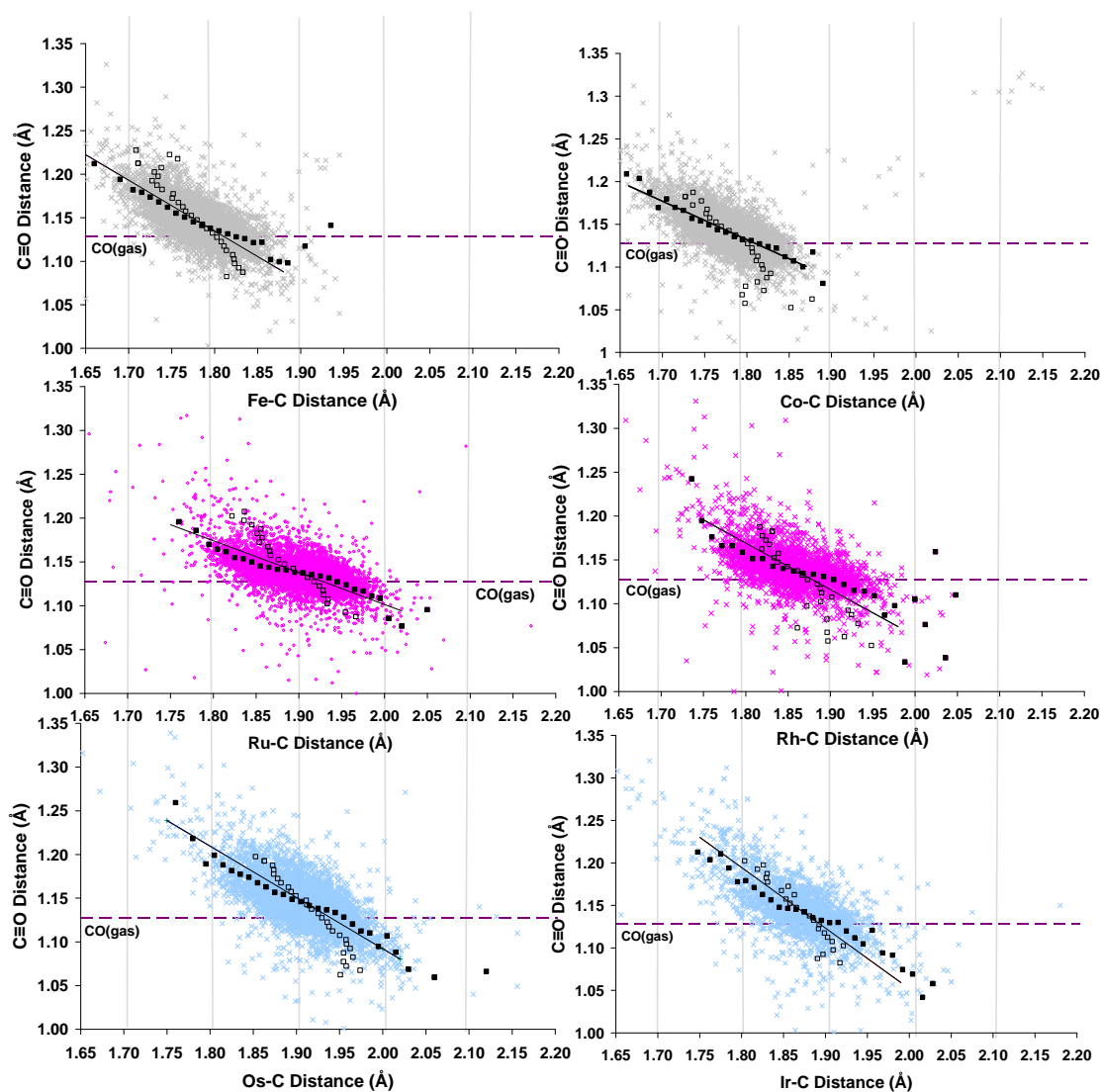


Figure S3. Scatter plot of C≡O distance vs. TM-C distance. Superposed are the weighted averages; the mean C≡O distance for a given TM-C distance $\{\bar{x}(C\equiv O|TM-C)\}$ (■), $\bar{x}(TM-C|C\equiv O)$ (□), and the principal component analysis (—), for groups 8 and 9. Grey lines are intended to reference the graphs to one another.

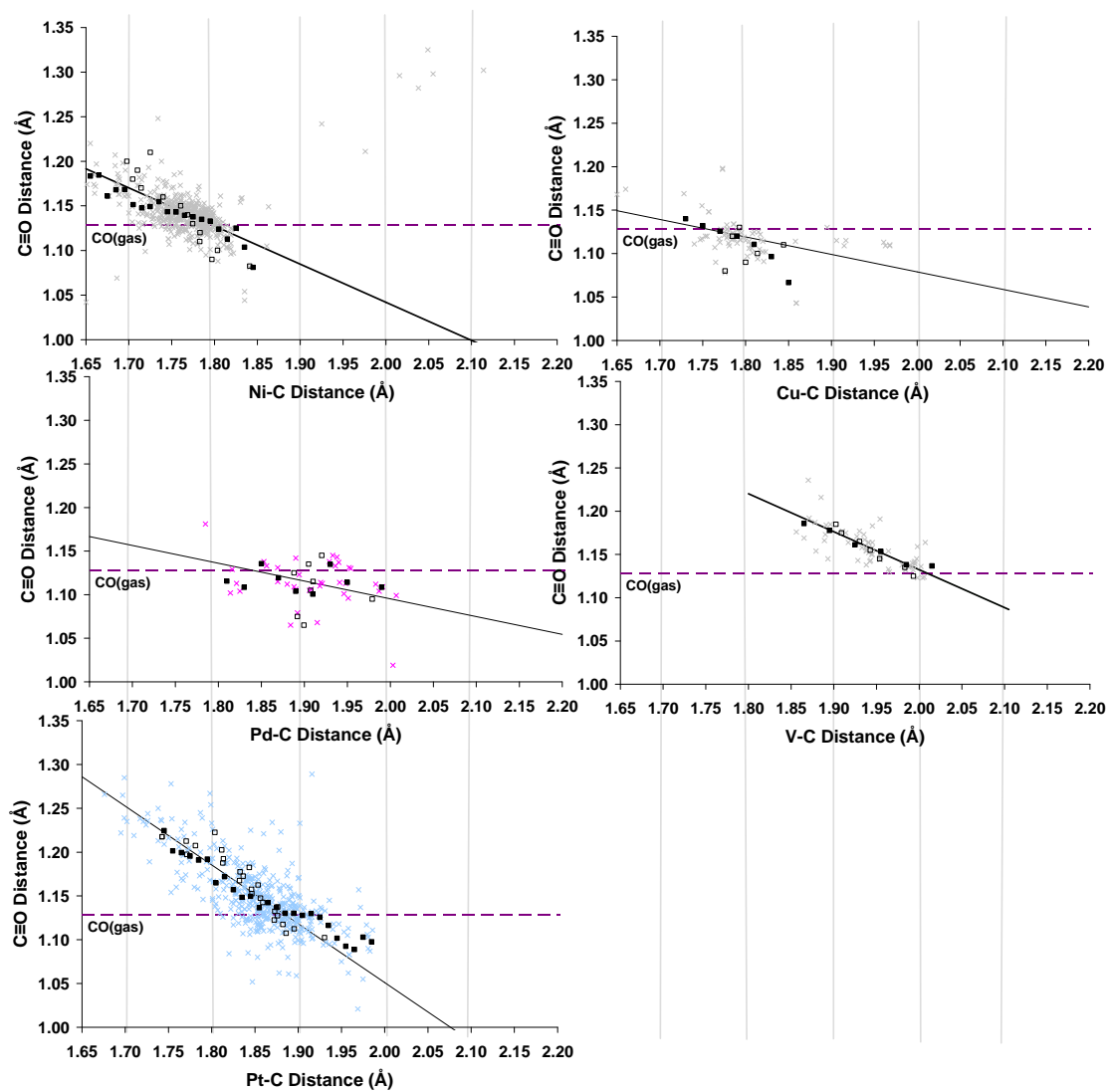


Figure S4. Scatter plot of C≡O distance vs. TM-C distance. Superposed are the weighted averages; the mean C≡O distance for a given TM-C distance $\{\bar{x}(C\equiv O|TM-C)\}$ (■), $\{\bar{x}(TM-C|C\equiv O)\}$ (□), and the principal component analysis (—) for group 10, vanadium and copper. Grey lines are intended to reference the graphs to one another.

Data sets given with the relative proportions of $\text{C}\equiv\text{O}$ distances at different points

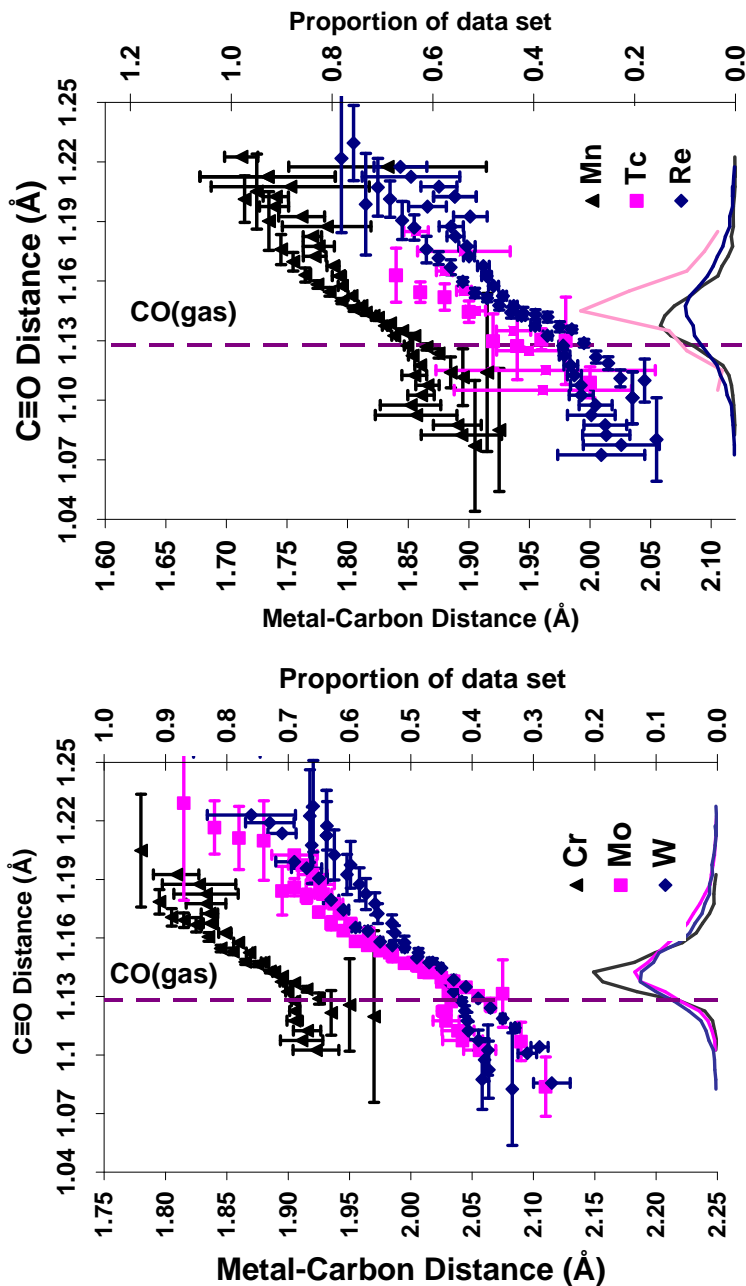


Figure S5. Curves representing the weighted average $\bar{x}(\text{C}\equiv\text{O}|\text{TM}-\text{C})$ and $\bar{x}(\text{TM}-\text{C}|\text{C}\equiv\text{O})$ of the relationship between TM-C and $\text{C}\equiv\text{O}$ bond lengths, for Groups 6 and 7.

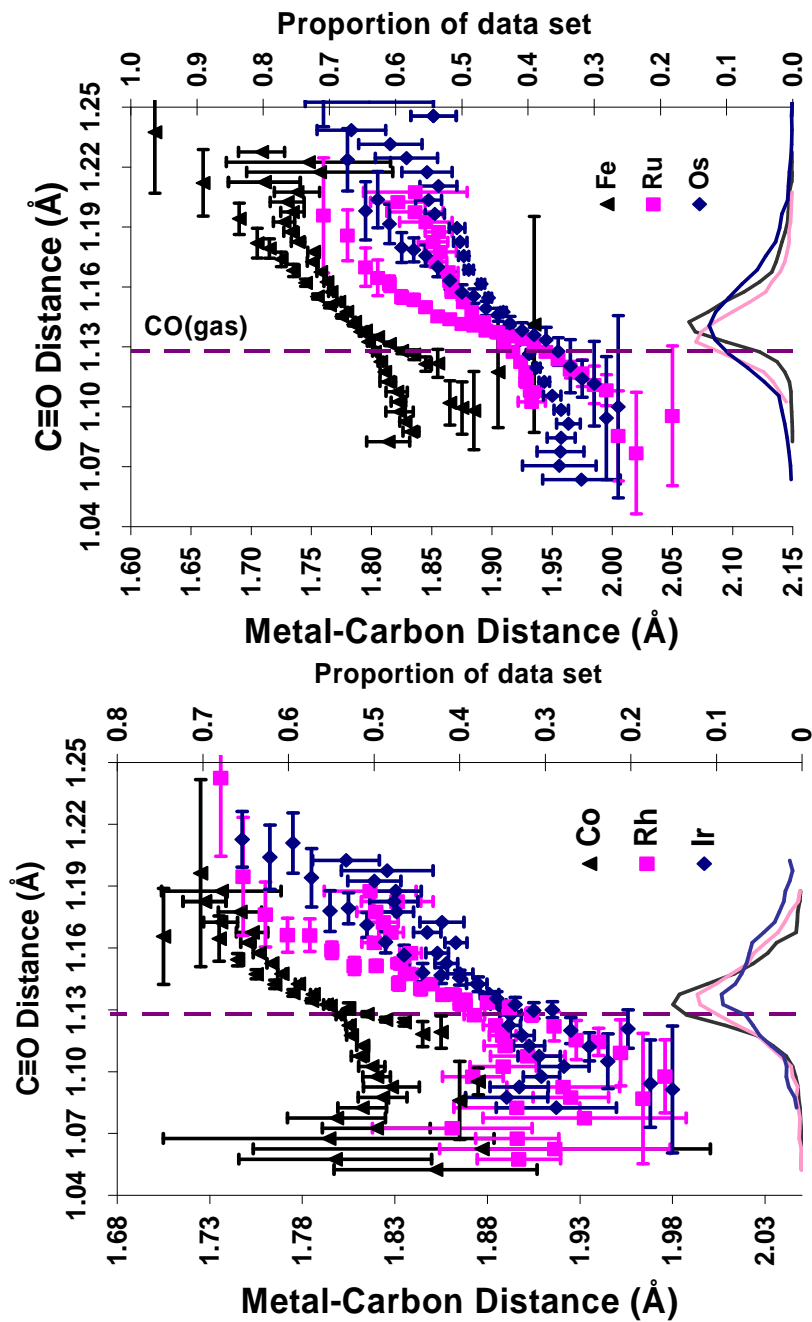


Figure S6 Curves representing the weighted average $\bar{x}(C\equiv O|TM-C)$ and $\bar{x}(TM-C|C\equiv O)$ of the relationship between TM-C and C≡O bond lengths, for Groups 8 and 9.

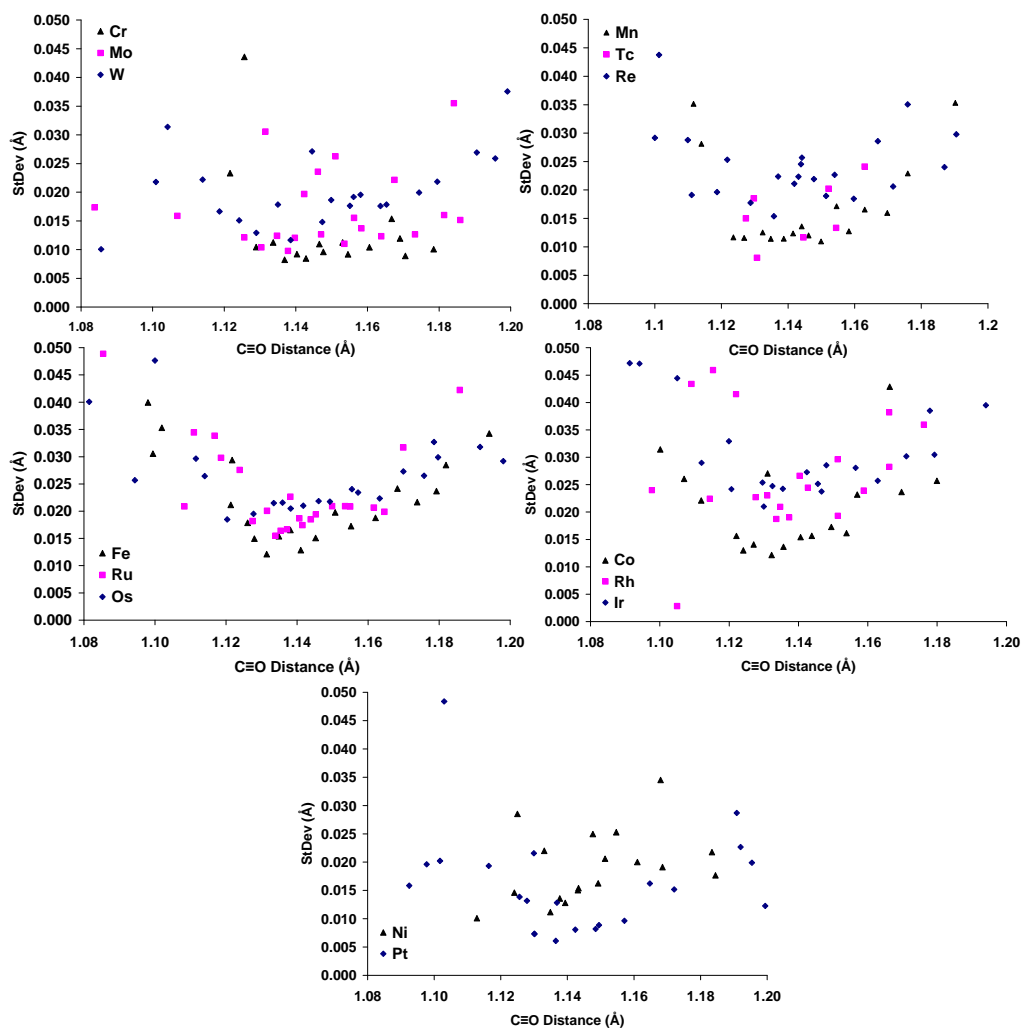


Figure S7. Scatter plots of the standard deviation on the groups of C≡O distances calculated in the analysis, \bar{x} (TM-C|C≡O), for Groups 6, 7, 8, 9 and 10.

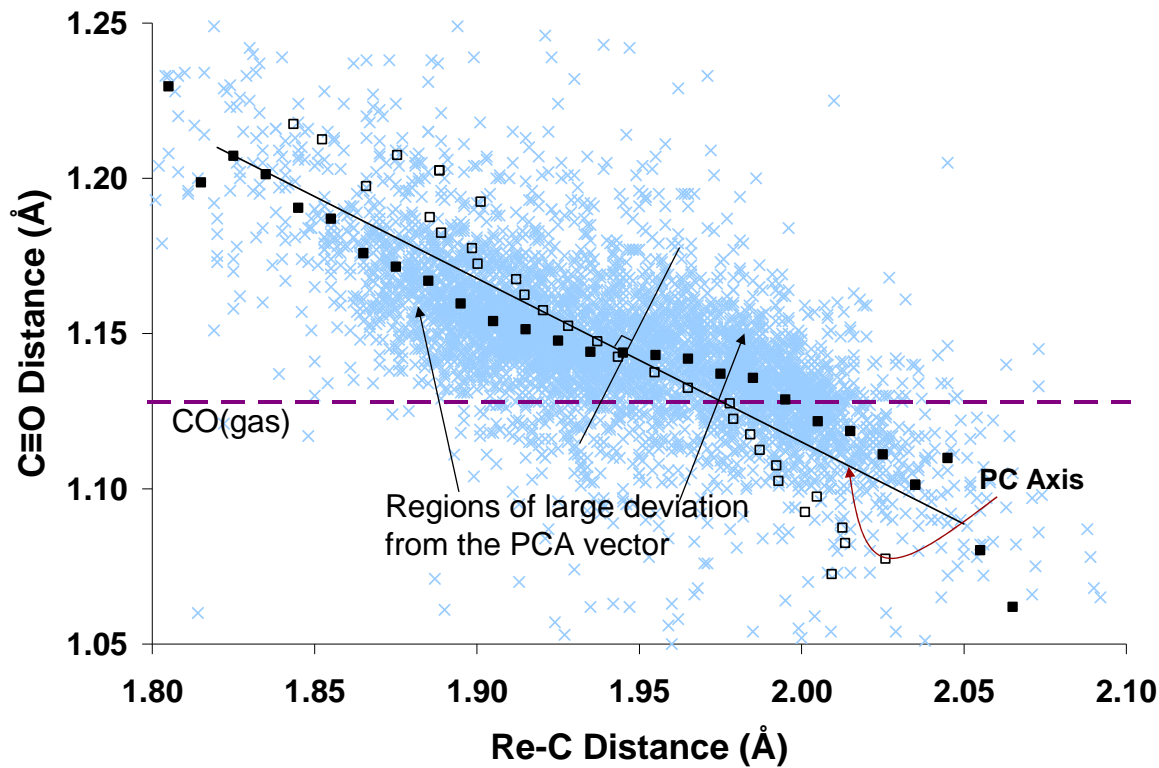


Figure S8. Scatter plot of C≡O distance *vs.* Re-C distance. Curves represent the weighted average: $\bar{x}(C\equiv O|Re-C)$ (■) and $\bar{x}(Re-C|C\equiv O)$ (□), and the principal component analysis (—) of the data. Arrows indicate regions where the data set deviates from the PC Axis.

Data plotted as 1st, 2nd and 3rd transition periods.

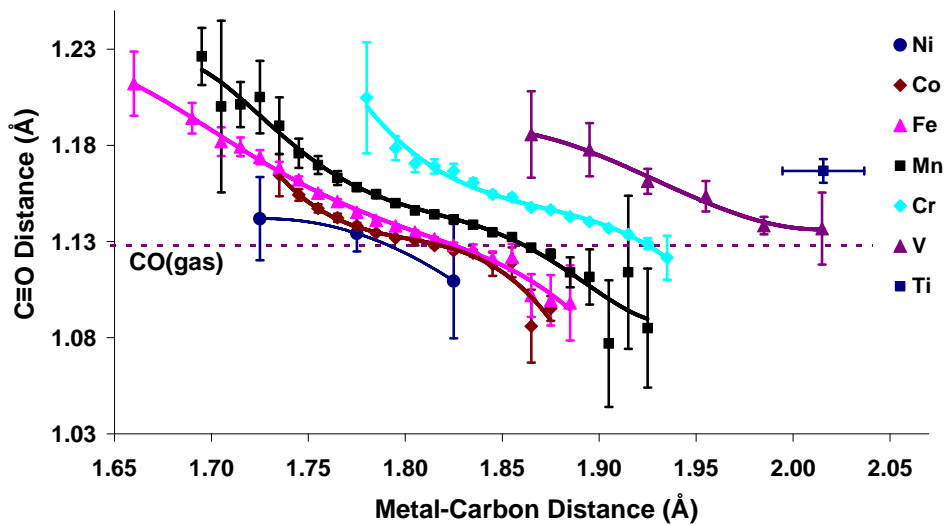


Figure S9. Plot of the mean C≡O distance for a given TM-C distance $\{\bar{x}(\text{C}\equiv\text{O}|\text{TM-C})\}$ (Å), for the sets of six-coordinate first-row transition-metal carbonyl complexes. Error bars represent the 95% confidence intervals on the mean, over the range for which the point is given. Data sets are based on the following numbers of *six-coordinate* TM-carbonyl interactions: Ni(175), Co(3,329), Fe(9,231) Mn(3,426), Cr(2,798), V(60), and Ti(5).

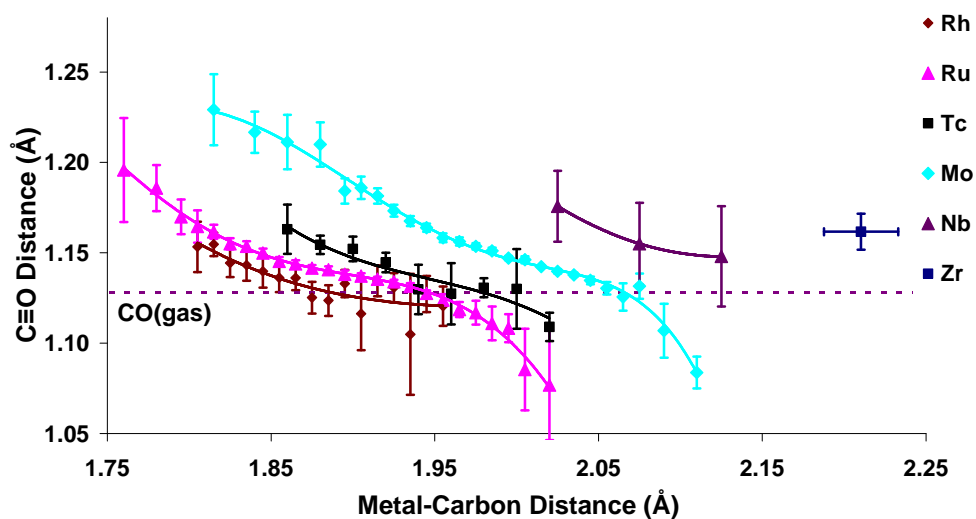


Figure S10. Plot of the mean C≡O distance for a given TM-C distance $\{\bar{x}(\text{C}\equiv\text{O}|\text{TM-C})\}$ (Å), for the sets of six-coordinate second-row transition-metal carbonyl complexes. Error bars represent the 95% confidence intervals on the mean, over the range for which the point is given. Data sets are based on the following numbers of *six-coordinate* TM-carbonyl interactions: Zr(3), Nb(9), Mo(3,240), Tc(118), Ru(6196) and Rh(244).

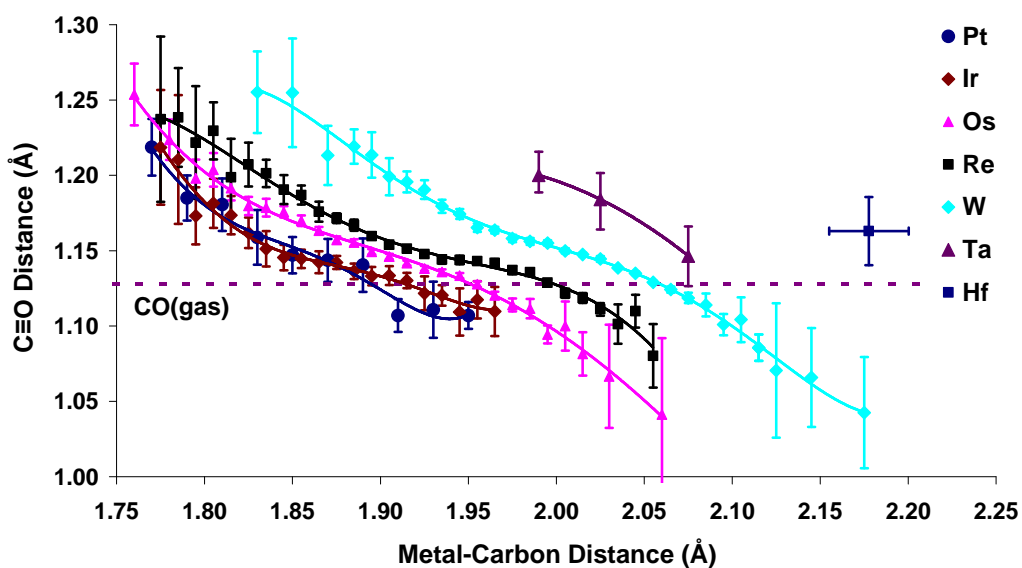


Figure S11. Plot of the mean C≡O distance for a given TM-C distance $\{\bar{x}(\text{C}\equiv\text{O}|\text{TM-C})\}$ (Å), for the sets of six-coordinate third-row transition-metal carbonyl complexes. Error bars represent the 95% confidence intervals on the mean, over the range for which the point is given. Data sets are based on the following numbers of six-coordinate TM-carbonyl interactions: Hf(3), Ta(13), W(6,202), Re(4,838), Os(6,552), Ir(857) and Pt(73).

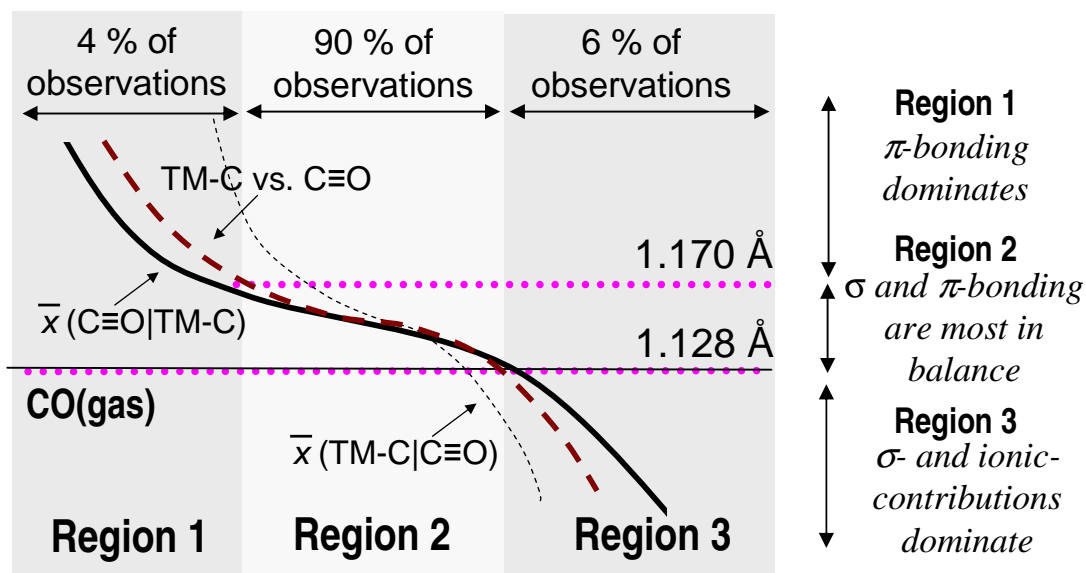


Figure S12. A schematic illustration based on Figures S3-S14, showing the regions where different types of bonding dominate and the type of bonding which dominates.

Analysis of Subsets.

Homoleptic TM-carbonyl species

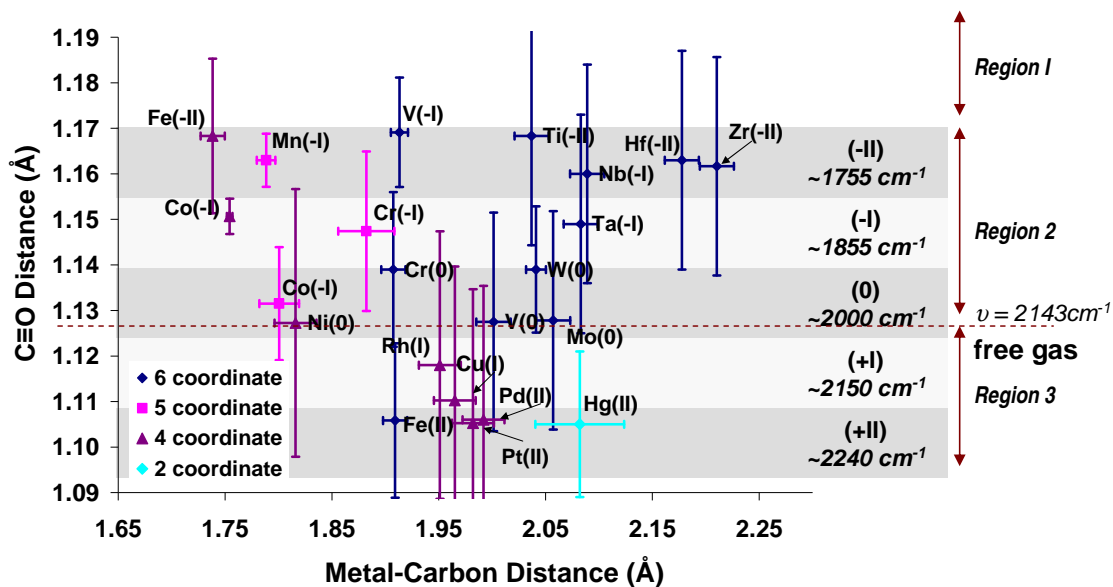


Figure S13 The structural data reported for homoleptic TM-carbonyl species illustrating the relationships between C≡O bond length, C≡O stretching frequency and metal oxidation.

The effect of other ligands in the coordination sphere

An example of a systematic change in the coordination sphere: the series



Table S1 shows the variation in Pt-C bond length originating from mutual ligand effects. The longest Pt-C bond lengths are observed in the species $[\text{Pt}(\text{CO})_4]^{2+}$ and the shortest in $[\text{PtCl}_3(\text{CO})]^-$, which is consistent with the carbonyl groups competing with one another, resulting in longer bond lengths.

Table S1. Structural data for the series of compounds $[\text{MCl}_n\text{CO}_{4-n}]^{2-n}$, M= Pt and Pd.

Species	Pt ^{II} -Cl Bond Length (Å)	Pt ^{II} -C Bond Length (Å)	C≡O Bond Length (Å)
$[\text{PtCl}_4]^{2-}$ (as §2.2.3)	2.303(0.002)	N/A	N/A
$[\text{PtCl}_3\text{CO}]^{-3}$	2.291	1.825	1.117
<i>cis</i> - $[\text{PtCl}_2(\text{CO})_2]^4$	2.292	1.897	1.115
$[\text{Pt}(\text{CO})_4]^{2+5}$	N/A	1.982	1.104
$[\text{PdCl}_4]^{2-}$ (as §2.2.3)	2.304(0.003)	N/A	N/A
$[\text{PdCl}_3\text{CO}]^{-6}$	2.289	1.869	1.115
$[\text{Pd}(\text{CO})_4]^{2+7}$		1.992	1.106

Analysis of trans ligands

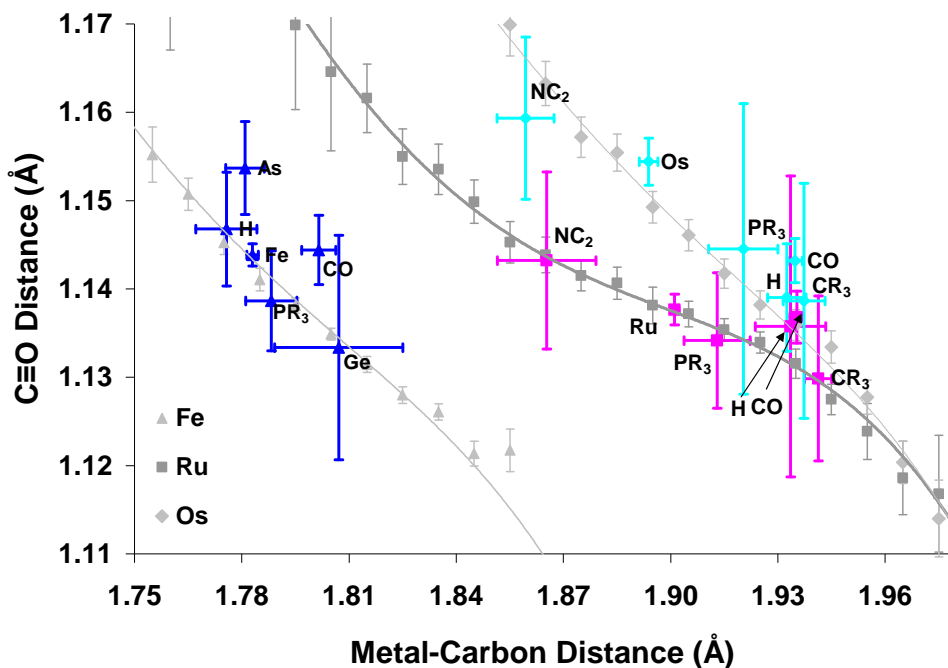


Figure S14. The average of subsets with different *trans*-donors for the group 8 metals.

The analysis described herein would be incomplete if no attempt was made to identify the effects of trans ligands and thereby consider the variation observed in TM-C bond lengths in terms of trans-effects. Figure S18 shows the average of data sets in which the donor trans to C≡O is the group indicated. From this data analysis the trans-influence series $\text{NR}_2 < \text{M} < \text{PR}_3 < \text{CR}_3 < \text{H} < \text{CO}$ is derived. This series is similar to that derived from TM-Cl bond lengths with the exception of carbon monoxide which appears at the opposite end of the series. This is not unexpected since TM-chloride and TM-carbonyl interactions have very different σ -bonding properties Cl is generally σ donor and CO is generally a π acceptor; thus making the two donors very different probes of trans influence.⁸⁻¹⁰

The effect of metal-metal bonds

From Figures S19 and S20 it is clear that compounds with M-M bonds dominate the Fe, Ru and Os datasets. This is not true of all datasets, see Table A4.4. The differences between the subsets containing no M-M bonds and the parent data set increase in the order Fe<Ru<Os. Removing compounds with M-M bonds increases the proportion of compounds in a high (>1) oxidation state from ~2% for Fe, 6% for Ru and 1.5% for Os to approximately 95%. Thus the changes evident in Figure S19 could be due to a wide variety of things including oxidation state, an alteration in the steric properties of the subsets or a contamination of incorrect structures.

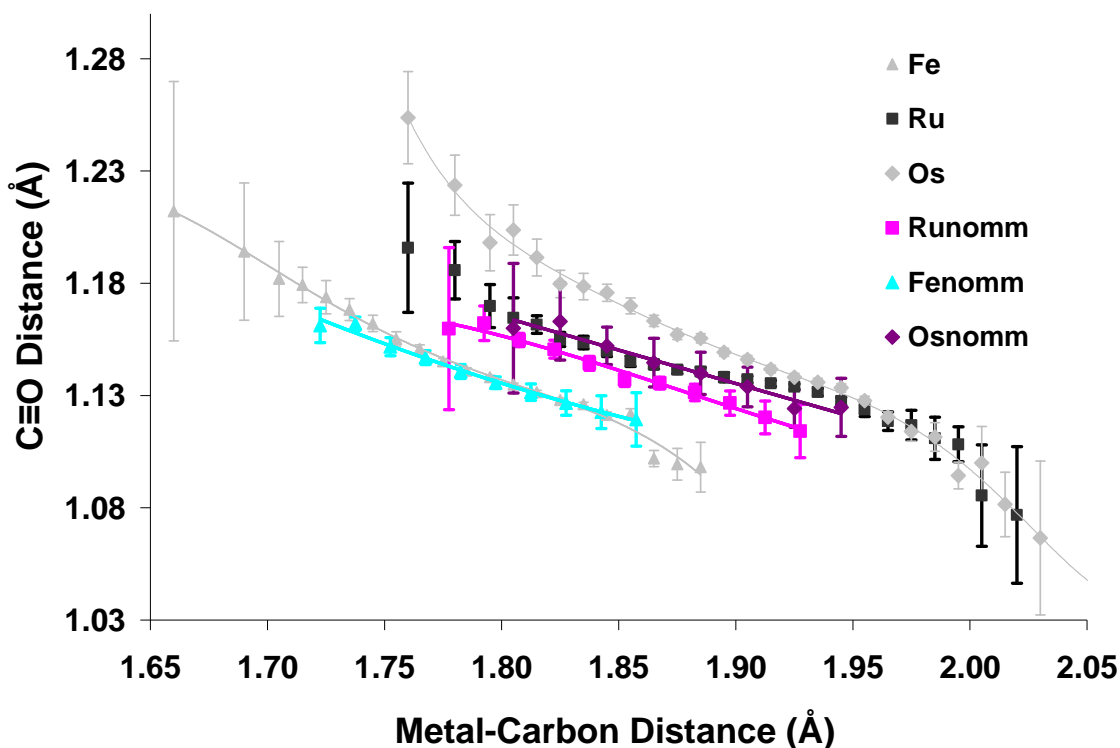


Figure S15. The effect of subtracting metal-metal bonds from the Fe, Ru and Os datasets; “nomm” indicates a subset with no metal-metal bonds.

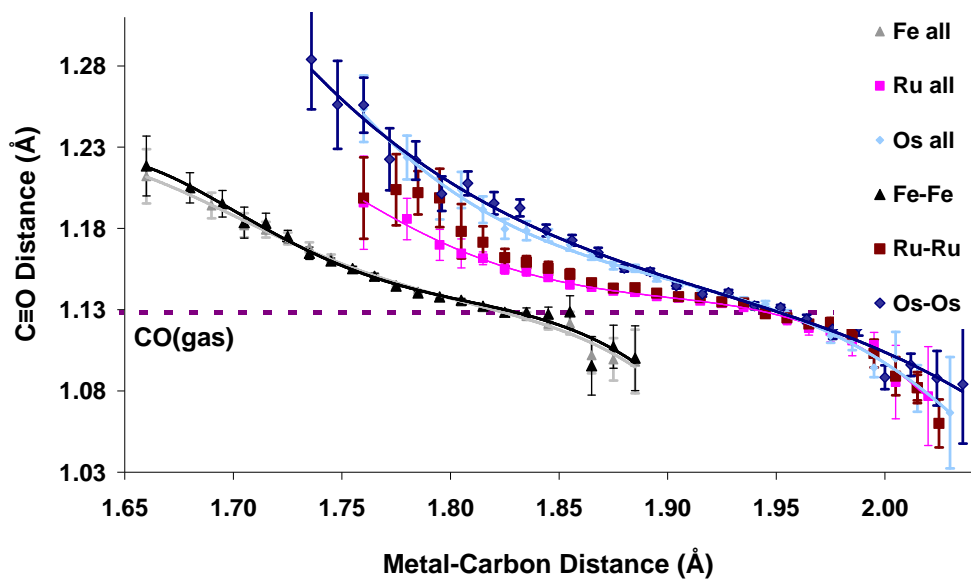


Figure S16. Comparison of the subsets of Fe, Ru and Os complexes containing a Fe-Fe, Ru-Ru or Os-Os bond respectively.

The effect of coordination number

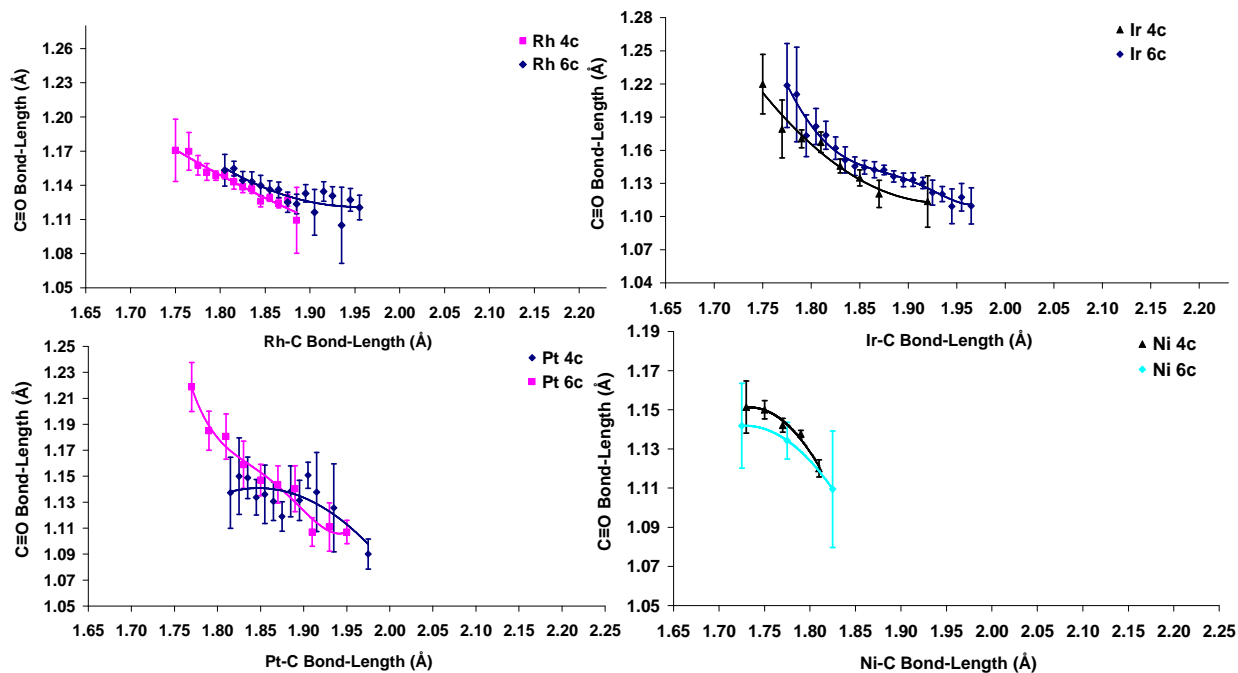


Figure S17. Comparison of the TM-C vs. C≡O relationships for different coordination numbers.

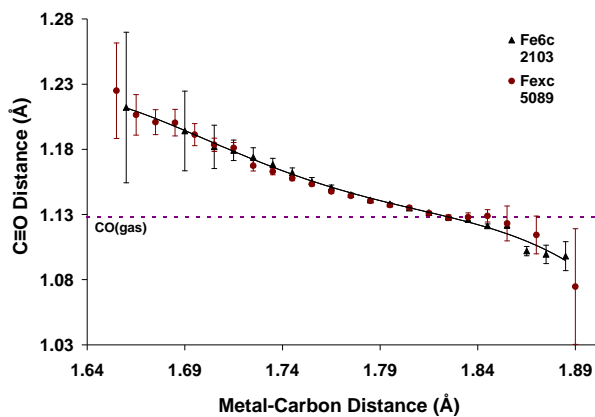


Figure S18. Comparison of the TM-C vs. C≡O relationship for 6 coordinate and all coordination numbers of the Fe-data set, with their relative numbers of structures.

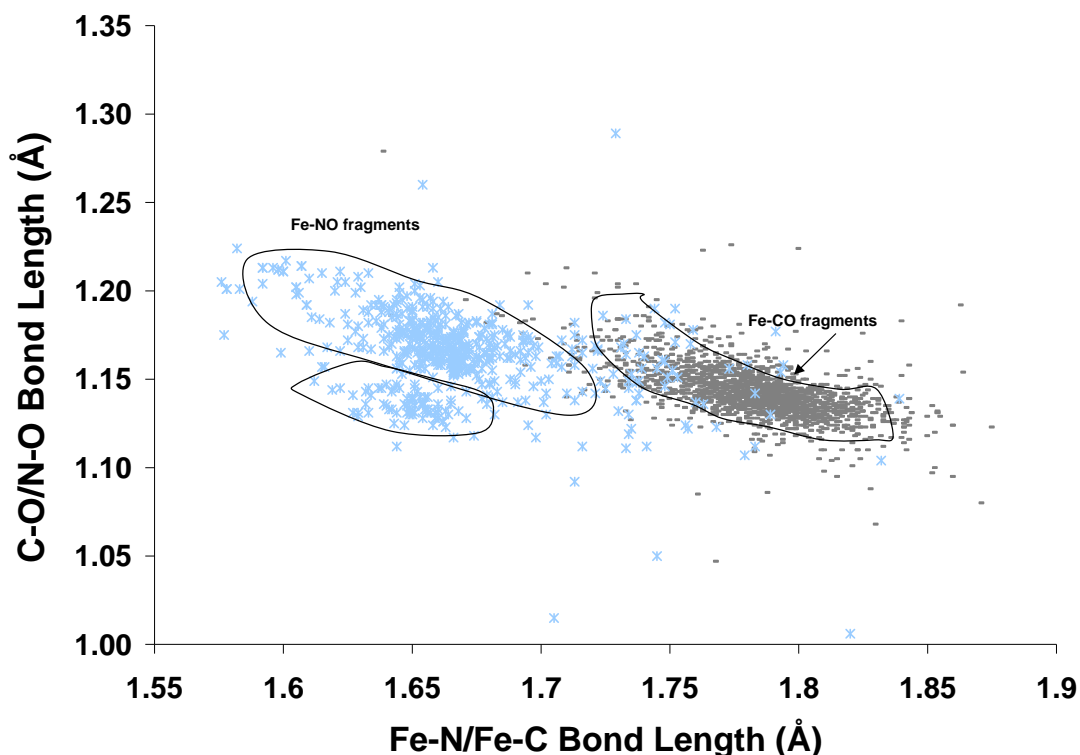


Figure S19. A Plot comparing Fe-NO fragments to Fe-CO fragments.

The Fe-CO fragments have 1 clear cluster of data, the Fe-NO fragments have 3 clear cluster of data, two are circled, a third superimposes the Fe-CO fragments.

- (1) Hocking R. K.; Hambley T. W. *Inorg. Chem.* **2003**, *42*, 2833-2835.
- (2) Hocking R. K.; Hambley T. W. *Dalton Trans.* **2005**, *5*, 969-978.
- (3) Russel D. R.; Tucker P. A.; Wilson S. J. *Organometallic Chem* **1976**, *104*, 387-389.
- (4) Bagnoli, F.; Dell' Amico, D. B.; Calderazzo, F.; Englert, U.; Marchetti, F.; Herberich, G. E.; Pasqualetti, N.; Ramello, S. *J. Chem. Soc., Dalton Trans.* **1996**, 4317-4318.
- (5) Willner, H.; Bodenbinder, M.; Broechler, R.; Hwang, G.; Rettig, S. J.; Trotter, J.; von Ahsen, B.; Westphal, U.; Jonas, V.; Thiel, W.; Aubke, F. *J. Am. Chem. Soc.* **2001**, *123*, 588-602.
- (6) Andreini B. P.; Dell' Amico, D. B.; Calderazzo F.; Venturi M. G. *J. Organomet. Chem.* **1988**, *354*, 369-380.
- (7) Willner H.; Bodenbinder M.; Brochler R.; Hwang G.; Rettig S. J.; Trotter J.; von Ahsen B.; Westpal U.; Jonas V.; Thiel W.; Aubke F. *J. Am. Chem. Soc.* **2001**, *123*, 588-602.
- (8) Goggin P. L.; Mink J. J. *Chem. Soc., Dalton Trans.* **1974**, 1479-1485.
- (9) Hartley F. R. *Chem. Soc. Rev.* **1973**, *2*, 163-189.

(10) Tobe M. L.; Burgess J. *Inorganic Reaction Mechanisms*; Addison Wesley Longman Limited: Edinburgh, 1999.